Pergamon

Acta mater. Vol. 46, No. 8, pp. 2683–2693, 1998

PII: S1359-6454(97)00477-1
1359-6454/98 $19.00 + 0.00

MODELLING DEFORMATION AND RECRYSTALLIZATION TEXTURES IN CALCITE

R. A. LEBENSOHN[1], H.-R. WENK[2] and C. N. TOMÉ[3]

[1]Instituto de Física Rosario (UNR-CONICET), 27 de Febrero 210 Bis, 2000 Rosario, Argentina,
[2]Department of Geology and Geophysics, University of California, Berkeley, CA 94720, U.S.A. and
[3]MST-8, MS G755, Los Alamos National Laboratory, Los Alamos, NM 87545, U.S.A.

(Received 29 August 1997; accepted 19 November 1997)

Abstract—A self-consistent polycrystal plasticity theory is applied to model the deformation and recrystallization behavior of rhombohedral calcite. In this mineral deformation occurs by slip and twinning and in experimentally deformed aggregates a strong crystallographic texture develops. Whereas the Taylor theory has failed to model axial compression, the self-consistent theory automatically introduces heterogeneous deformation by curling and simulates the correct texture. A deformation-based recrystallization model, that balances growth and nucleation, predicts a so far enigmatic high temperature texture. Aspects of mechanical twinning are also discussed. Many of the conclusions are directly applicable to other low-symmetry materials, especially hexagonal metals. © *1998 Acta Metallurgica Inc.*

1. INTRODUCTION

Deformation of calcite $CaCO_3$ (trigonal symmetry, spacegroup $R\bar{3}c$), and calcite rocks such as limestone and marble has long been a subject of experimental and theoretical investigations. Deformation mechanisms established in single crystal experiments [1, 2] have then been used to predict the development of preferred orientation during large strain deformation. A first qualitative attempt was introduced in the Yule marble studies done by Turner *et al.* [3] by applying the model of Calnan and Clews [4]. Taylor's polycrystal plasticity theory was used as a basis for quantitative modelling of calcite deformation textures [5–7]. Results of such modelling has been applied to interpret deformation histories from texture patterns, including sense of shear and strain partitioning [8–10].

Success with these models has been mixed. It was possible to reproduce general texture patterns in calcite rocks deformed in plane strain [6] but the Taylor theory failed to explain textures in axially deformed limestone, both in compression and extension [11]. This has been attributed to locally heterogeneous deformation, not readily incorporated in the Taylor theory which assumes compatibility. Another difficulty has been the modelling of deformation twinning which is easily activated in calcite [12]. Furthermore, there has been no satisfactory interpretation of the experimentally observed recrystallization texture [13].

More recently, selfconsistent polycrystal plasticity theories have been introduced [14, 15] which allow for heterogeneous deformation according to the relative local anisotropy. These models were successfully applied to a number of low-symmetry materials, such as hexagonal zircaloy [15], trigonal quartz [16], and orthorhombic olivine [17]. Also the modelling of twinning reorientation and its role in texture development was the matter of detailed studies, in some cases in combination with selfconsistent models [18]. Finally, the heterogeneous local deformation provided by these models were used in the formulation of a deformation-based recrystallization model [19]. The combination of all these recent modelling advances provides new insights into the fundamental mechanisms of texture development in low-symmetry materials.

In this paper we use the most recent version of the visco plastic self consistent (VPSC) code [20] which handles deformation by twinning and accounts for the full anisotropy of the polycrystal. This VPSC code, which also incorporates Wenk *et al.* [19] recrystallization model, is applied to calcite in order to explain deformation textures and texture development during dynamic recrystallization. The study reveals some fundamental concepts of polycrystal plasticity modelling and results from this complex system with low crystal symmetry and a variety of slip and twinning systems that are also relevant for other low symmetry materials, including metals. Simulation results are compared with experiments which displayed some features that could not be explained up to now.

Figure 1 shows three texture patterns, produced in axial compression experiments and represented as inverse pole figures, that have been difficult to interpret [13]. At low temperature, where mechanical twinning dominates over slip, a broad maximum of compression axes near (0001) is observed (Fig. 1(b)). At intermediate temperature and low

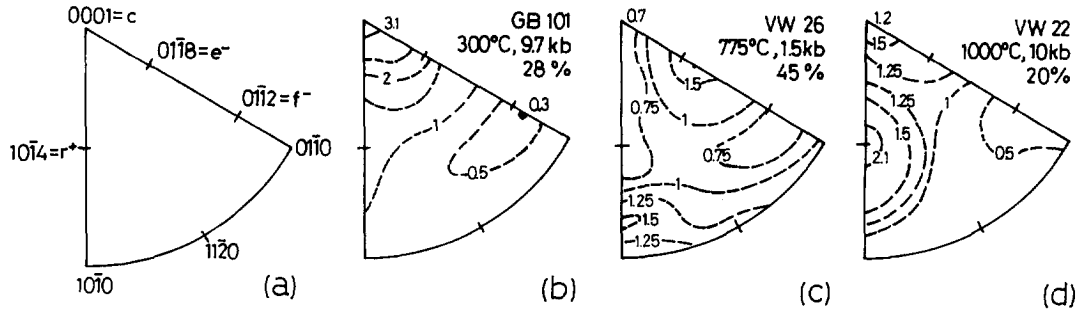

Fig. 1. Experimental deformation of calcite limestone in axial compression. (a) Schematic of main crystallographic orientations and symbols. Inverse pole figures (in equal area projection) for (b) low temperature, (c) high temperature, (d) high temperature with recrystallization and grain growth [13].

confining pressure, as slip on rhombs is active, the maximum shifts towards negative rhombs, near (01$\bar{1}$8) (Fig. 1(c)). At high temperature and high confining pressure the microstructure documents recrystallization with grain growth and the texture shows a maximum of compression axes near high angle positive rhombs (10$\bar{1}$4) (Fig. 1(d)). We will use the VPSC model to provide plausible interpretations for these texture patterns, based on the relative importance and mutual influence between deformation by slip and twinning and recrystallization by nucleation and growth.

2. MODEL

Real polycrystalline materials deform in the ductile range by maintaining local stress equilibrium and strain compatibility. This is achieved through local variations from grain to grain and even within grains. However, such a situation is extremely difficult to model, even with the most sophisticated finite element formulations presently available [21] and, instead, simplifications have been used. At one extreme is the model of Taylor which assumes homogeneous deformation throughout the polycrystal, regardless of crystal orientation. At the other extreme is the concept of Sachs which assumes equilibrium and sacrifices compatibility. Corrections to these models have been introduced such as the "relaxed constraints" Taylor model [22] and the modified Sachs model [23].

Unlike the different Taylor and Sachs variants, the viscoplastic selfconsistent formulation allows the local stress and strain-rate to be different from the corresponding macroscopic magnitudes, according to their directional plastic properties. The VPSC model — in its 1-site [15], 2-site [24] and *n*-site [25] approximations — has been widely used for the prediction of deformation textures and described in detail. Therefore, we will not present here the complete formulation but only the most relevant equations of the 1-site approach, together with the scheme for twinning reorientation and the VPSC-based recrystallization model.

If the geometry and critical stresses of the active slip and twinning systems in each grain are known, the local strain-rate is given by the viscoplastic equation:

$$\dot{\varepsilon}^g = \sum_s m^{s,g}\dot{\gamma}^{s,g} = \dot{\gamma}_o \sum_s m^{s,g}\left(\frac{m^{s,g}:\sigma'^g}{\tau_c^{s,g}}\right)^n \qquad (1)$$

where $m^{s,g}$, $\dot{\gamma}^{s,g}$ and $\tau_c^{s,g}$ are the Schmid tensor, the shear-rate and the critical stress of the slip or twinning system (s); $\dot{\gamma}_o$ is a reference strain-rate and n is the inverse of the rate-sensitivity.

Basically, the VPSC model consists in regarding each grain of the polycrystal as a viscoplastic inclusion deforming in an viscoplastic homogeneous effective medium (HEM). This medium has the average properties of the polycrystal and is based on the determination of the interaction tensor $\tilde{M}$, given by:

$$\tilde{M} = n(I - S)^{-1}:S:M^{(\mathrm{sec})} \qquad (2)$$

where S is the viscoplastic Eshelby tensor [15] which depends on the grain shape and the plastic properties of the HEM and $M^{(\mathrm{sec})}$ is the secant macroscopic compliance which is not known *a priori* but it has to be determined selfconsistently. This interaction tensor relates the deviations in stress and strain-rate from where it is possible to get the local states. The interaction tensor depends both explicitly and implicitly (via the Eshelby tensor) on the macroscopic modulus. The latter can be determined imposing that the averages of stress and strain-rate over all the grains have to be consistent with the corresponding macroscopic magnitudes.

A texture development calculation is carried out by imposing incremental steps of deformation. After each step, the critical stresses of each deformation system and the orientation and shape of the grains is updated. The critical stresses are updated via a microscopic hardening law of the type:

$$\dot{\tau}_c^{s,g} = \sum_{s'} h^{ss'}\dot{\gamma}^{s',g} \qquad (3)$$

where $h^{ss'}$ is a microhardening matrix and the

shear-rates $\dot{\gamma}^{s',g}$ can be obtained from equation (1). In order to update the orientation of the grains, different kinds of lattice rotations should be considered. In addition to the macroscopic and local plastic rotations (due to sample rotation, slip activity, and grain shape effects), twinning is an additional source of reorientation and therefore of texture development. When a twin is formed inside a crystal, some volume fraction of it adopts a completely different but crystallograhically related orientation.

Several schemes have been proposed to deal with the effect of twinning reorientation in texture development [15, 26, 27]. On the one hand, the volume fraction transfer (VFT) scheme [15] is an eulerian scheme that keeps track of the exact twinned fraction using a fixed grid in Euler space and variable volume fractions, rather than following the reorientation of individual grains. VFT produces good predictions when twinning controls texture development but the lack of individual orientations prevents from any further application of a deformation-based recrystallization model. The predominant twin reorientation (PTR) scheme [27], on the other hand, requires some approximations to treat the twinned fraction but captures the main role of twinning reorientation in texture development and, at the same time, keeps the identity of individual grains, including their properties. For this reason, the PTR is a better candidate to be implemented inside a VPSC code that has to handle plastic anisotropy, twinning reorientation and recrystallization.

Briefly, the PTR scheme consists in keeping track of three magnitudes associated with twinning, namely: (a) $F^{s,g}$: the volume fraction of each twin system (s) inside each grain (g), given by the accumulated shear associated with that twin divided by the characteristic twin shear, (b) F^{tot}: the sum of the individual $F^{s,g}$ over all systems and grains and (c) F^{eff}: the effective twinned fraction, given by the grains reoriented according to the random selection described below. If F^{eff} is less than F^{tot} a random choice of a grain (g) is made. A complete reorientation by twinning of the randomly-selected grain is performed if the following condition is fulfilled in one of the twinning systems:

$$F^{s,g} > 0.25 + 0.25 \times \frac{F^{eff}}{F^{tot}}. \tag{4}$$

In this way, reorientation by twinning takes place in those systems with the highest twinning activity in the grain, but not before at least 25% of the original grain fraction has been transformed by twinning. As the accumulated twinned fraction F^{tot} growths larger than the effective twinned fraction F^{eff}, the second term of the sum in the right decreases and further reorientation by twinning is favored until F^{eff} "catches up". In this way, both fractions tend to remain approximately equal throughout deformation, which means that the whole grain is reoriented when about 50% of the grain volume has transformed via the "predominant" twin system. The thresholds of 25% and 50% are arbitrary, but changing these numbers within reasonable limits has little effect on the final texture.

In the VPSC formulation some orientations deform more than others leading to large variations in strain and therefore in stored strain energy. Based on the VPSC model and assuming that the stored strain energy in the grains dominates recrystallization, Wenk *et al.* [19] proposed a deformation-based recrystallization model for low-symmetry materials. From this model, highly strained grains are likely to recrystallize by nucleation or to disappear through invasion by neighbors. Thus, the recrystallization texture is due to a balance between nucleation and the boundary mobility that makes a grain shrink or grow. It is acknowledged that this recrystallization model inherits an intrinsic limitation from the 1-site VPSC deformation model on which it is based: it assumes that the strain and the strain energy are homogeneously distributed inside the grains. This means that the development of intragranular sources of misorientation and stress concentration (i.e.: potential sites for nucleation of recrystallization) like dislocation structures, twin boundaries, shear bands, etc. is not considered by this model. Nevertheless, making an adequate choice of the nucleation and growth parameters, the model predictions show good agreement with textures observed in experimentally and naturally deformed and recrystallized geological materials, like halite, quartz and ice. The basic equations of the recrystallization model are (see Ref. [19]):

2.1. Nucleation

$$E^{g,(k)} = E_0 \sum_s (\tau_c^{s,g,(k)} - \tau_c^{s,g,(0)})^2 \tag{5}$$

$$B^{(k)} = \beta \times \max_g E^{g,(k)} + (1 - \beta) \times \min_g E^{g,(k)} \tag{6}$$

$$P^{g,(k)} = \begin{cases} \exp[-A/(E^{g,(k)})^2] & \text{if } E^{g,(k)} > B^{(k)} \\ 0 & \text{if } E^{g,(k)} < B^{(k)} \end{cases} \tag{7}$$

where $E^{g,(k)}$ and $\tau_c^{s,g,(k)}$ are the stored energy and the critical stress of system (s) in grain (g) after deformation step (k), E_0 is a normalization factor to give units of energy, β is a number between 0 and 1 that defines a threshold energy for nucleation $B^{(k)}$ after step (k). A is the nucleation parameter (in units of energy square), and $P^{g,(k)}$ is the actual probability of a nucleation event after step (k), between 1 and 0.

2.2. Growth

$$\dot{w}^{g,(k)} = C \times (\bar{E} - E^{g,(k)}) \times (w^{g,(k)})^{2/3} \qquad (8)$$

where $w^{g,(k)}$ is the volume fraction (with respect to the whole polycrystal) of grain (g) in step (k), $\dot{w}^{g,(k)}$ is the rate of change of that fraction, C is the growth parameter (in inverse units of energy) and $\bar{E}$ is the average strain energy over all grains.

3. DATA PROCESSING AND MATERIAL PARAMETERS

One of the outputs from polycrystal plasticity calculations is the final texture, given as a set of individual orientations defined by Euler angles with weights representing the volume fraction of the grain. Other parameters used to characterize the heterogeneous deformation are the equivalent stress and strain for each grain and, in the case of dynamic recrystallization, a marker that indicates whether the grain has nucleated or not, or whether it has grown, shrunk or disappeared.

For axial compression geometry an inverse pole figure is the most effective way to represent preferred orientation. All information can be represented in an azimuthal sector of 60°, spanning from $(10\bar{1}0)$ to $(01\bar{1}0)$. In what follows, some inverse pole figures represent individual orientations ("grains") directly, assigning different symbol sizes and symbol types. Other figures use contour plots. The latter were obtained by calculating first a continuous orientation distribution (OD) from individual orientations, placing a spherical Gauss function of 10° width on each orientation. From the OD, the inverse pole figure was calculated and plotted. For all this data manipulation and representation computer programs contained in the Berkeley texture package [28] were used.

Two different cases were investigated in order to find a relationship between the observed variation of textures with temperature as illustrated in Fig. 1. On one hand, we investigated the influence of relative critical stresses for the different deformation mechanisms on texture. On the other hand, we assumed the same "deformation texture" by using the same set of critical stresses, and studied the effect of recrystallization parameters.

Largely based on experiments on single crystals, deformation mechanisms in calcite have been determined [1]. Mineralogists traditionally have assigned letters to crystal faces for abbreviation. In the case of calcite deformation (0001) is referred to as c, $(10\bar{1}4)$ as r, $(01\bar{1}8)$ as e and $(01\bar{1}2)$ as f. Slip has been observed on two rhombs (r and f) and, particularly at low temperature, mechanical twinning (e^-) is prevalent. Typical combinations of relative critical stresses for low (LT), intermediate (IT), and high (HT) temperature, obtained by interpolation of experimental values, are summarized in Table 1. This list reflects the following experimental features: while the critical stresses for slip decrease with temperature, the ones for twinning are more difficult to assess because twinning depends on local stress concentrations [2]. Provided that stress concentrations are more likely at low temperature, a lower critical stress is associated with twinning at low temperature relative to slip. As temperature increases, we assume that the gap between r^- and r^+ increases while f^- slip becomes relatively softer than the r slip modes.

Table 1. Deformation mechanisms in calcite and their critical stresses (arbitrary units), adopted for low, intermediate and high temperature

Mode	LT	IT	HT
r^- slip $\{10\bar{1}4\}\langle 20\bar{2}1\rangle$	1.0	1.0	1.0
r^+ slip $\{10\bar{1}4\}\langle \bar{2}021\rangle$	1.6	2.0	2.0
f^- slip $\{\bar{1}012\}\langle 0\bar{2}2\bar{1}\rangle$	1.6	1.0	0.5
e^+ twinning $\{\bar{1}018\}\langle 40\bar{4}1\rangle$	0.4	0.8	2.0

In order to check our hypothesis that dynamic recrystallization causes texture changes, we assumed LT deformation conditions and controlled dynamic recrystallization by assigning different values to the parameters A, β and C (equations (5)–(8)). Although these parameters are related to microscopic mechanisms like stress concentrations, misorientations, grain boundary energy, etc, we do not make any attempt to compute them *ab-initio*. Instead, we check that the parameters selected reflect a reasonable dynamics of the recrystallization process (e.g.: the grains shrink or grow smoothly and, after each deformation step, the nucleation events occur in a few of the most deformed grains).

Two recrystallization cases were explored: (a) when dynamic recrystallization is dominated by the growth of grains due to boundary mobility and nucleation can be disregarded, (b) when both nucleation and growth are operative and affect the final texture. It is obvious from equations (5)–(8) that for high A the occurrence of nucleation is prevented, while for small C the occurrence of growth is prevented. Table 2 shows the selected A, β and C.

Concerning other model parameters, the strain rate sensitivity has been determined in creep experiments with polycrystals. A stress exponent of $n = 9$ is applicable for a regime of dislocation glide and climb [29]. Only at high temperature and low pressure, fine-grained limestone deforms superplastically with a much higher rate sensitivity and no

Table 2. Recrystallization parameters A, β and C for $E_0 = 1$ (A, C and E_0, arbitrary units, consistent with the units of the critical stresses). See also equations (5)–(8)

Growth	Nucleation and growth
A high	$A = 0.0001$
	$\beta = 0.7$
$C = 3000$	$C = 3000$

development of preferred orientation [30]. We assumed a uniform stress exponent $n = 9$ for all slip and twinning systems. For the microscopic hardening, an isotropic hardening law was imposed of the form:

$$h^{ss'} = 0.1 \times \tau_c^s \quad \text{(for arbitrary s')}. \tag{9}$$

The calcite aggregate was represented using a set of 1000 randomly generated orientations. All the orientations were assigned the same initial weight and the same initial equiaxed grain shape. All the simulations were carried out up to a Von Mises equivalent strain of 30% in 15 deformation increments of 2%, to match approximately the deformation associated with the experimental textures in Fig. 1. Grain shape, orientation and relative weight are updated as deformation and recrystallization proceed.

4. RESULTS

4.1. Deformation

The inverse pole figures displayed in Fig. 2 correspond to a viscoplastic Taylor and self-consistent deformation calculations for the low, intermediate and high temperature conditions stated in Table 1, but suppressing the growth and nucleation mechanisms. For the Taylor case (right column in the figure) the inverse pole figures display a maximum of compression axes at a high angle positive rhomb. This is similar to earlier Taylor calculations [11] but does not conform with experiments showing that, with increasing temperature, the maximum displaces from near (0001), towards low angle negative rhombs and, eventually, towards high angle positive rhombs (Fig. 1).

Self-consistent simulations produce distinctly different textures with a (0001) maximum at LT, a maximum at low angle negative rhombs at IT and a similar pattern, but with the maximum located at a higher angle, at HT (Fig. 2, left column). The first transition from low to intermediate temperature is in good agreement with the experiments (see Fig. 1) but the model does not reproduce the high temperature texture with a maximum at high angle positive rhombs.

Dashed and solid lines in Fig. 3 show the relative activity of slip and twinning systems in the FC and SC cases, respectively. These relative activities were obtained by normalizing and averaging the shears associated with each deformation system, inside each grain. Despite some quantitative differences in the activities, predicted by the FC and SC models, both calculations give the same expected qualitative trend, i.e.: the e^+ twinning activity decreases while the f^- slip activity increases with temperature. Thus it is not the difference in slip system activity that causes the differences in the texture patterns obtained with the two models. As will be explained in the next section, the explanation for the differences between the FC and SC results requires a detailed analysis of the local strain heterogeneities.

4.2. Recrystallization

In the case of dynamic recrystallization the critical stresses for LT (see Table 1) were assumed, which lead to the texture displayed in Fig. 4(a) in the absence of nucleation and/or growth. Two cases were considered: if nucleation is suppressed and *growth dominates*, the texture which develops shows a maximum near a high angle positive rhomb (Fig. 4(b)), in good agreement with the observed HT texture (Fig. 1(d)). In case of *balanced growth and nucleation* the main maximum is at (0001) (Fig. 4(c)).

Figure 5 shows other relevant data from the growth-controlled recrystallization simulation. Figure 5(a) shows a map of vanished grains (diamonds) and non-vanished grains (crosses). The vanished grains represent 36.7% of the initial set of grains and their orientation is largely concentrated around (0001). These grains, with the $\langle c \rangle$-axis near the compression direction, are the most deformed ones and therefore are invaded by other grains with plastically harder orientations. The symbol size in Fig. 5(b) is proportional to the magnitude of the accumulated strain. The smallest symbol represents 0.22 and the largest symbols 0.69, in equivalent strain units. Grains with large symbols in Fig. 5(b) (e.g. those near (0001), but also others) correlate perfectly with those that have disappeared due to grain boundary migration (Fig. 5(a)). Finally, the main features of the final texture can be visualized in Fig. 5(c) in which the symbol size is proportional to the final volume fraction of individual grains. The largest symbols represents 7 times the initial (uniformly distributed) volume fraction of the grains. The symbols of the vanished grains are obviously missing. In this final distribution, a few big grains are located at high angle positive rhombs and more numerous but smaller grains are found at low angle negative rhombs. This explains the observed high temperature texture in calcite (Fig. 1(d)).

Figure 6 shows some features of the predicted textures and microstructures when nucleation is active. Squares in Fig. 6(a) correspond to those grains that have nucleated at some stage of the deformation process. As expected, the higher density of nucleated grains corresponds to the highly deformed orientations, near (0001). In contrast to the growth dominated case, the plastically soft grains (large symbols in Fig. 6(b)) nucleate and the stored energy is reset to zero. After the nucleation event they grow, giving a persistent (0001) maximum, and they may nucleate again. As a consequence, after 30% deformation only 1% of the grains vanished and the largest grains are smaller

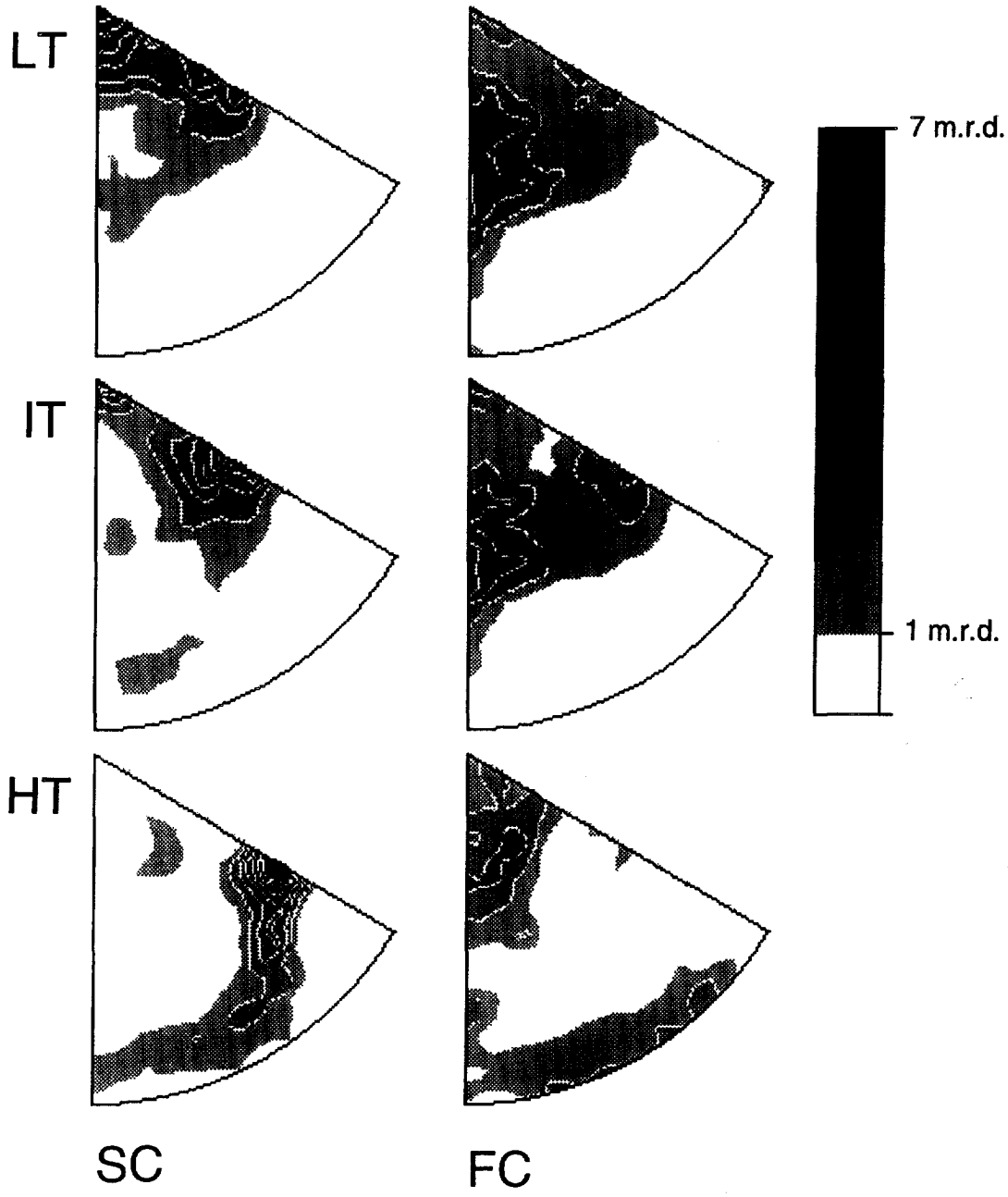

Fig. 2. Texture simulations of calcite in axial compression after 30% strain, represented as inverse pole figures of the compression direction, for LT, IT and HT (see also Table 1). The contoured inverse pole figures are based on plasticity simulations of 1000 grains done with the viscoplastic self-consistent theory (left side) and the full constraints Taylor theory (right side).

than in the former case (3.2 times the initial volume fraction, Fig. 6(c)).

5. DISCUSSION

The viscoplastic self-consistent polycrystal plasticity theory applied to calcite is able to explain textural and microstructural features that could not be reproduced with the Taylor model. This mineral system, with low crystal symmetry and rather complex deformation mechanisms has been very useful to illustrate some of the features and advantages of the SC model. We will discuss briefly some implications for heterogeneous deformation, mechanical twinning and dynamic recrystallization.

5.1. Heterogeneous deformation

It has been noted previously that Taylor simulations reasonably predict plane strain textures of calcite but fail for axial compression and extension [11]. The observed texture resembles the plane strain (pure shear) texture, averaged about

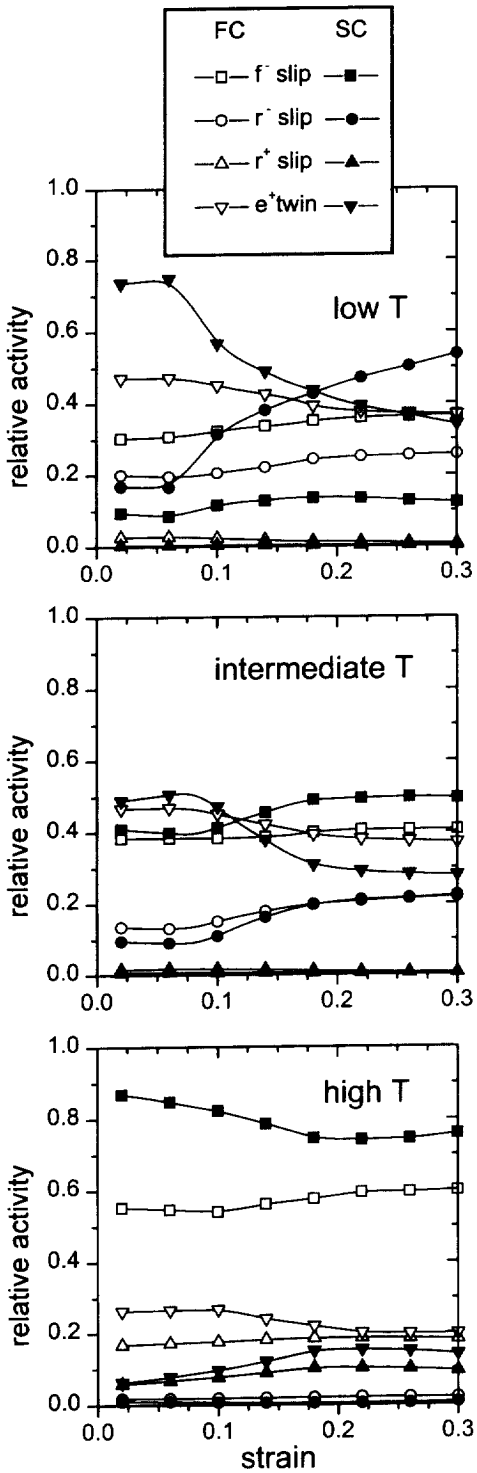

Fig. 3. Relative activity of slip and twinning systems during compressive deformation of calcite, as predicted with the self-consistent model (solid symbols) and the Taylor theory (open symbols).

the compression direction. It was interpreted as an effect called "curling", observed in axially compressed b.c.c. metals where individual grains do not deform in the applied axial symmetry but in plane strain, and strain heterogeneity is accommodated by bending and twisting [31]. Whereas the full constraints Taylor theory requires homogeneous deformation, curling can be introduced by relaxing $d\varepsilon_{22}-d\varepsilon_{11}$ and $d\varepsilon_{12}$ so that each crystal can freely choose two of its principal strain directions normal to the compression direction [11]. Such relaxation, though, is difficult to justify on the basis of grain-shape arguments.

In the self-consistent formulation the likelihood of curling is implicit if this mechanism is energetically favorable. In order to assess this possibility we have investigated the grain shape distribution and plotted a histogram of the principal axes of the ellipsoids that represent each grain. Figure 7 shows the statistics of the individual grain shape for the case IT (no recrystallization) after 30% compression. a_1, a_2 and a_3 denote the short, intermediate and long axes respectively of the ellipsoids that represent the grains. The SC calculation predicts a broad distribution with three rather than two maxima as one would expect for axisymmetric compression and pancake-shaped grains. In the FC case, on the other hand, a_1 and $a_2 = a_3$ are the same for all the 1000 grains in the texture. In the SC case there is an expected dispersion (since the local deformations are non homogeneous). While for the short axis, the maximum of the SC distribution is very close to the ideal FC value, the distributions of a_2 and a_3 in the SC case are far removed from the FC value. The intermediate and the long axis distributions are clearly bimodal. The center of the intermediate axis distribution is only slightly larger than 1, indicating that locally the grains are close to a plane strain condition. However, although individually the grain deformations depart from axisymmetric conditions, their average value reproduces the axially symmetric deformation of the aggregate.

5.2. *Mechanical twinning*

As shown in the previous section, reorientation by twinning plays an important role in the development of low temperature deformation textures and also provides highly deformed orientations that subsequently affect the evolution of recrystallization textures. Therefore, the reliability of the twinning reorientation scheme must be assessed. Figure 8 shows the performance of the PTR twinning scheme used together with the SC model at low temperature. As discussed in Section 2, the effective twinned fraction F^{eff} (i.e.: the sum of the volume fractions of the grain actually reoriented by twinning) should remain as close as possible to the total twinned fraction F^{tot} (i.e.: the sum of the twinned fractions for all twinning systems and for all the grains) throughout the calculation. As shown in Fig. 8, there is an initial transient stage in which the individual twinned fractions $F^{s,g}$ were too small to fulfill condition (4) followed by a good and stable

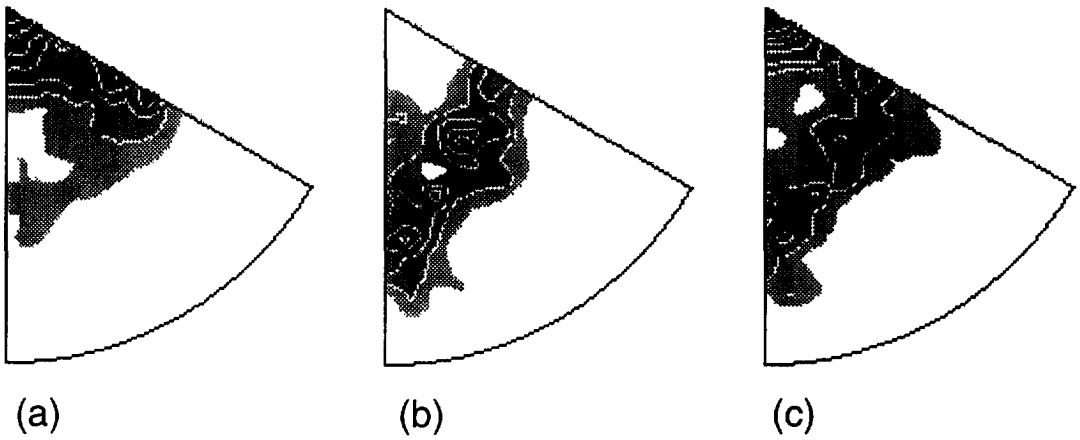

Fig. 4. Texture predictions of calcite in axial compression after 30% strain with accompanying dynamic recrystallization (see also Table 2) (a) only deformation, (b) growth-controlled case and (c) balanced growth and nucleation.

match between the effective and the total twinned fractions.

Figure 9 analyzes the influence of the plasticity model on twinning. Open and solid symbols correspond to calculated accumulated twinned fractions for the FC and the SC model respectively, at different temperatures. The FC predictions are appreciably higher, particularly at high temperature when the twinning systems are relatively harder than the slip systems. This rather "insensitive" behavior of the Taylor theory to changes in the relative critical stresses of the deformation modes has been reported for hexagonal metals [15, 18] and is due to the fact that the activation of hard systems is necessary in order to fulfill the imposed conditions. This also explains why the FC results do not show appreciable changes for different temperatures (i.e.: for different combinations of critical stresses).

5.3. Dynamic recrystallization

The results of the simulations demonstrate that for low and intermediate temperature deformation of calcite, an adequate model for slip and twinning can explain experimental data, as long as local plastic anisotropy is taken into account. The prediction of high temperature textures requires, in addition, a reliable deformation-based model to account for dynamic recrystallization effects. In this case, the model provides not only predictions of textures but also gives valuable information about the microstructures that must be necessarily associated with those textures.

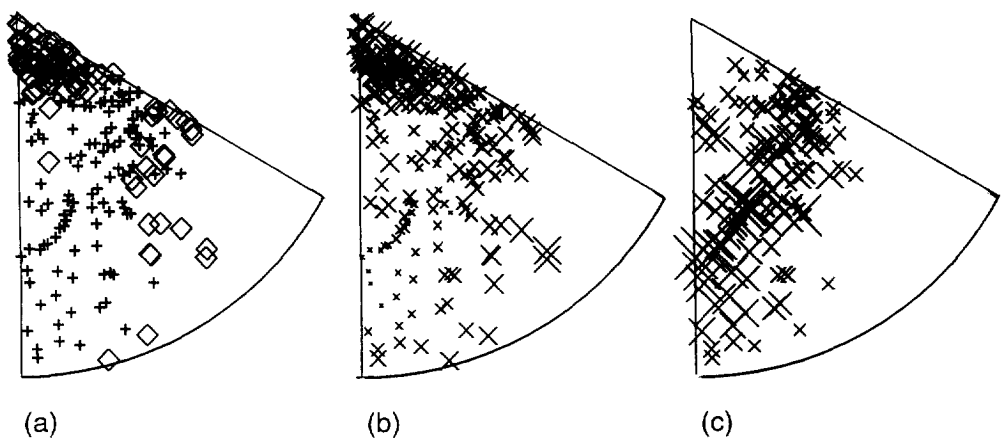

Fig. 5. Inverse pole figures with individual orientations, illustrating features during growth-controlled recrystallization after 30% compression. (a) Map of vanished grains (diamonds) and non-vanished grains (crosses). (b) Effective strain, symbol size is proportional to magnitude: smallest symbols represent 0.22 and largest symbols 0.69, in equivalent strain units. (c) Volume fraction of individual grains, largest symbols represents 6.66 times the initial volume fraction.

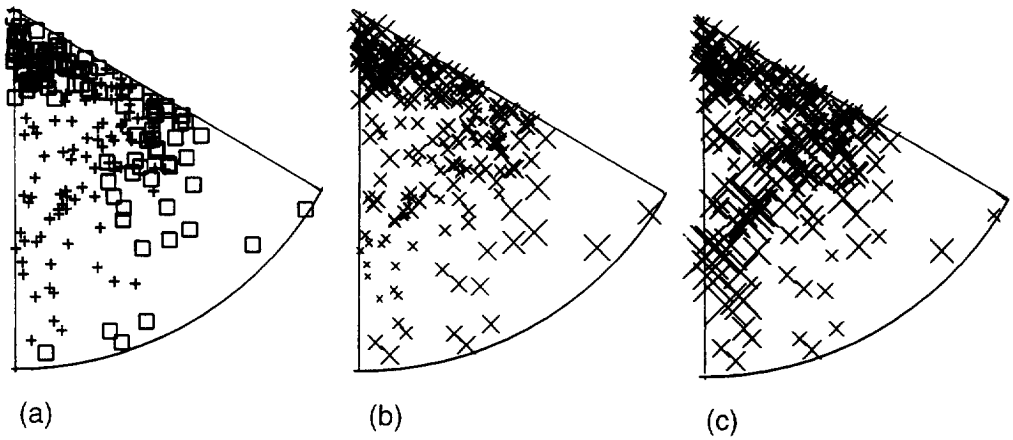

Fig. 6. Inverse pole figures with individual orientations, illustrating features in a regime of balanced nucleation and growth recrystallization after 30% compression. (a) Map of nucleated grains (squares) and non-nucleated grains (crosses). (b) Effective strain, symbol size is proportional to magnitude: smallest symbols represent 0.15 and largest symbols 0.68, in equivalent strain units. (c) Volume fraction of individual grains, largest symbols represents 3.75 times the initial volume fraction.

In the growth-controlled case the model predicts a texture with a compression axis maximum at high angle positive rhombs which is exactly what is observed experimentally (Fig. 1(c)) in samples where grain size increased by an order of magnitude (from < 5 to 30 μm, Fig. 10(a), (b)). Meanwhile, the deformation map of individual grains documents that the orientations near $(10\bar{1}4)$ are roughly seven times larger than the initial uniform grain size (Fig. 5(c)) and three times less deformed than those orientations near the c-axis (0001) (Fig. 5(b)). It is therefore plausible that, as long as nucleation is suppressed, these "hard" grains would grow at the expense of other orientations and dominate the recrystallization texture.

If nucleation is active the situation becomes more complicated. The most highly deformed grains near (0001) will nucleate, become strain free and ultimately consume the less deformed non-nucleated grains. Up to now there is no experimental example of such a texture but a texture pattern with c-axes near the compression direction is the most common

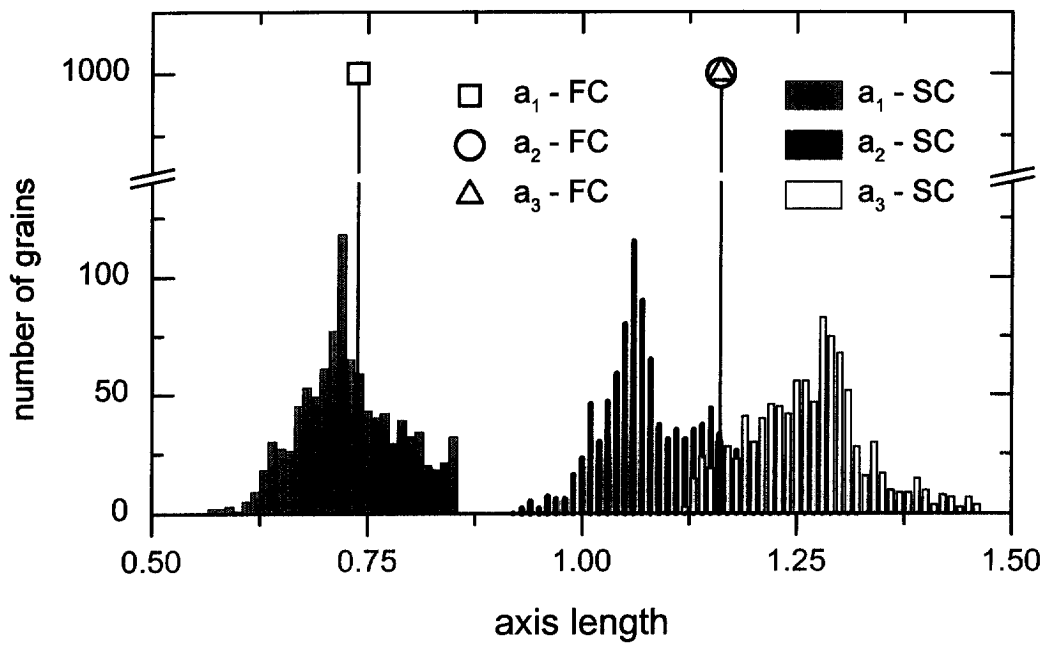

Fig. 7. Statistical distribution of grain axes for case IT (no recrystallization) after 30% compressive deformation, predicted with Taylor and SC models.

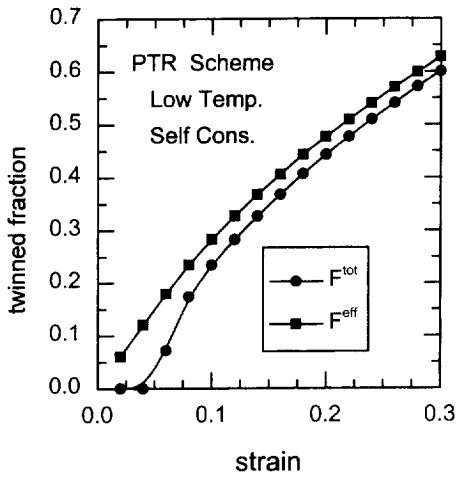

Fig. 8. Performance of the predominant twinning reorientation (PTR) scheme during compressive deformation of calcite. Case LT, SC model.

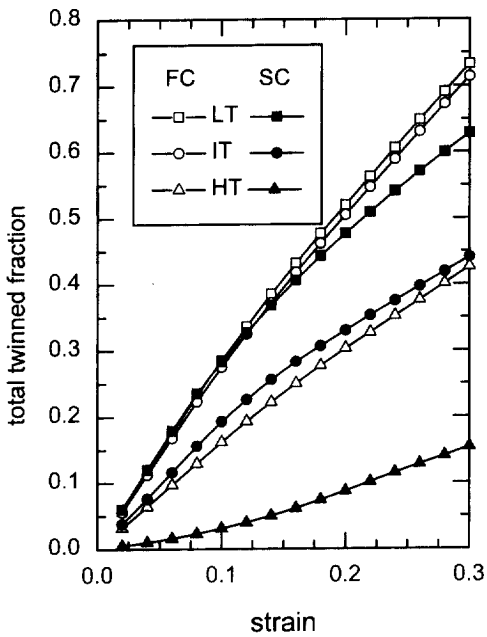

Fig. 9. Evolution of the twinned fraction during compressive deformation of calcite as predicted with the self-consistent (solid symbols) and the Taylor (open symbols) models.

type in naturally deformed marbles [10, 32]. In these samples, small grains surrounding a large old twinned grain document that nucleation plays an important role (Fig. 10(c)).

It should be mentioned that recrystallization simulations were done with LT deformation conditions in which twinning is active. One reason for this was to separate the effects of changing critical shear stresses and recrystallization parameters. For the growth-controlled case different deformation textures lead to a similar recrystallization texture since grains with compression axes near $(10\bar{1}4)$ are hardest. In the case of nucleation it is necessary to have orientations near (0001) and these are produced by twinning. In naturally deformed and recrystallized carbonate rocks twins are always present (e.g. Figure 10(c)). In fact nucleation often

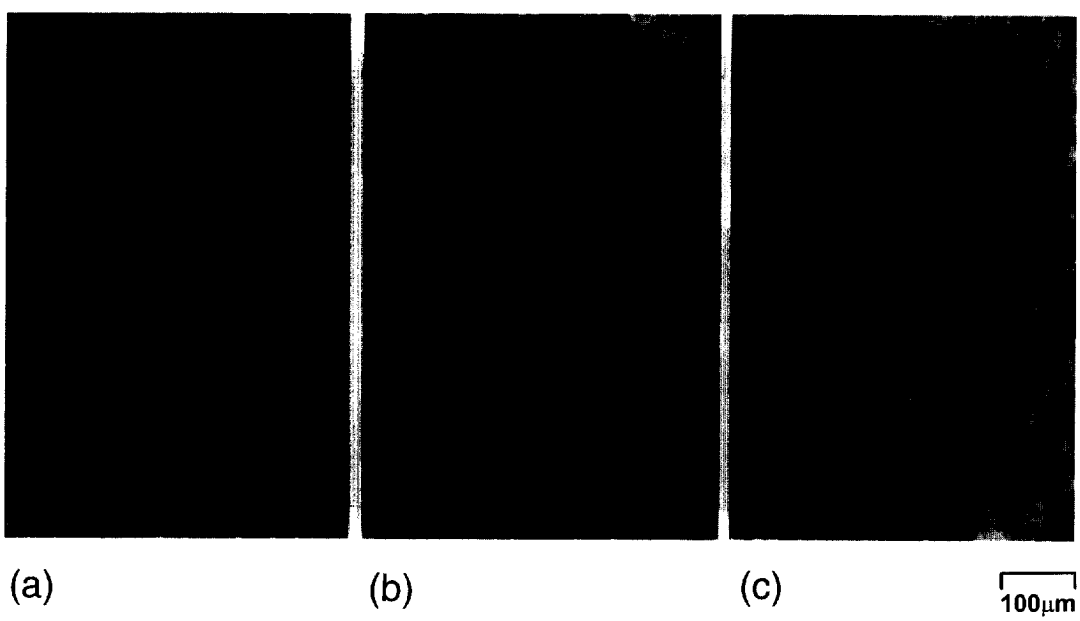

Fig. 10. (a) Micrograph of the microstructure of the starting limestone material. (b) After experimental recrystallization with significant grain growth [13]. (c) In deformed natural marbles recrystallization by nucleation is often observed [10]. Scale is the same for all the micrographs.

begins on twin planes. These recrystallized marbles are often coarse-grained and it has been observed that twinning and associated texture changes are more prevalent in coarse marbles than in fine-grained limestones [33].

6. CONCLUSIONS

The examples in this paper illustrate that the 1-site viscoplastic self-consistent theory is a flexible approach to model plasticity of heterogeneous, anisotropic and low-symmetry systems. Orientation-dependent heterogeneous deformation is accounted for automatically, without having to introduce rather arbitrary conditions of relaxed constraints in the Taylor framework. Texture and microstructure are predicted and can be directly compared with experiments. The model handles twinning with a proper balance of the actual and effective twin fractions. Since a record is kept of individual grain deformation, the model is easily modified for dynamic recrystallization and can predict textures during growth and nucleation. The deformation of calcite has been a good example to highlight these properties of the viscoplastic self-consistent model which is also directly applicable to materials of engineering interest.

Acknowledgements—One of us, R.A.L., wishes to acknowledge the Fulbright Program for providing the fellowship during which period this work took place, and also the Center for Materials Science (Los Alamos National Laboratory) for hosting him during two weeks. A grant from NSF (EAR 94-17580) and IGPP-LANL supported this research.

REFERENCES

1. Turner, F. J., Griggs, D. T. and Heard, H. C., *Bull. Geol. Soc. Am.*, 1954, **65**, 883.
2. DeBresser, J. P. H. and Spiers, C. J., *Tectonophysics*, 1997, **272**, 1.
3. Turner, F. J., Griggs, D. T., Clark, R. H. and Dixon, R. H., *Geol. Soc. Am. Bull.*, 1956, **67**, 1259.
4. Calnan, E. A. and Clews, C. J. B., *Philics. Mag.*, 1950, **41**, 1085.
5. Lister, G. S., *Proc. 5th. Int. Conf. on Textures of Materials*, Vol. 2, ed. G. Gottstein and K. Lucke, 1978, p. 199.
6. Wagner, F., Wenk, H.-R., Van Houtte, P. and Esling, C., *Contrib. Mineral. Petrol.*, 1982, **80**, 132.
7. Takeshita, T., Tomé, C. N., Wenk, H.-R. and Kocks, U. F., *J. Geophys. Res.*, 1987, **B92**, 12917.
8. Wenk, H.-R., Takeshita, T., Bechler, E., Erskine, B. G. and Matthies, S., *J. Struct. Geol.*, 1987, **9**, 731.
9. Ratschbacher, L., Wenk, H.-R. and Sintubin, M., *J. Struct. Geol.*, 1991, **13**, 369.
10. Erskine, B. G., Heidelbach, F. and Wenk, H.-R., *J. Struct. Geol.*, 1993, **15**, 1189.
11. Wenk, H.-R., Kern, H., Van Houtte, P. and Wagner, F., *Am. Geoph. U. Monogr.*, 1986, **36**, 287.
12. Tomé, C. N., Wenk, H.-R., Canova, G. R. and Kocks, U. F., *J. Geophys. Res.*, 1991, **B96**, 11865.
13. Wenk, H.-R., Venkitasubramanyan, C. S., Baker, D. W. and Turner, F. J., *Contrib. Mineral. Petrol.*, 1973, **38**, 81.
14. Molinari, A., Canova, G. R. and Ahzi, S., *Acta metall.*, 1987, **35**, 2983.
15. Lebensohn, R. A. and Tomé, C. N., *Acta metall. mater.*, 1993, **41**, 2611.
16. Wenk, H.-R., Canova, G. R., Molinari, A. and Kocks, U. F., *J. Geophys. Res.*, 1989, **B94**, 17895.
17. Wenk, H.-R., Bennett, K., Canova, G. R. and Molinari, A., *J. Geophys. Res.*, 1991, **B96**, 8337.
18. Lebensohn, R. A. and Tomé, C. N., *Mater. Sci. Engng A*, 1994, **175**, 71.
19. Wenk, H.-R., Canova, G. R., Brechet, Y. and Flandin, L., *Acta mater.*, 1997, **45**, 3283.
20. Lebensohn, R. A. and Tomé C. N., to be published.
21. Sarma, G. B. and Dawson, P. R., *Acta mater.*, 1996, **44**, 1937.
22. Honneff, H. and Mecking, H., *Proc. Sixth Int. Conf. on Texture of Materials*, The Iron and Steel Institute of Japan, Tokyo, 1981, p. 347.
23. Leffers, T., *Strength of Metals and Alloys*, ed. P. Haasen, V. Gerold and G. Kostorz, Pergamon, Oxford, 1979, p. 769.
24. Lebensohn, R. A. and Canova G. R., *Acta mater.*, 1997, **45**, 3687.
25. Canova, G. R., Wenk, H.-R. and Molinari, A., *Acta metall. mater.*, 1992, **40**, 1519.
26. Van Houtte, P., *Acta metall.*, 1978, **26**, 591.
27. Tomé, C. N., Lebensohn, R. A. and Kocks, U. F., *Acta metall.*, 1991, **39**, 2667.
28. Wenk, H.-R., Matthies, S. S., Donovan, J. and Chateigner, D., *J. appl. Crystallogr*, 1998, in press.
29. Heard, H. C. and Raleigh, C. B., *Geol. Soc. Am. Bull.*, 1972, **83**, 935.
30. Schmid, S. M., Boland, J. N. and Paterson, M. S., *Tectonophysics*, 1977, **43**, 257.
31. Hosford, W. F., *Trans. metall. Soc. A.I.M.E.*, 1964, **230**, 12.
32. Trommsdorff, V., *Schweiz. Mineral. Petrog. Mitt.*, 1964, **44**, 495.
33. Kern, H., *Bull. Minéral.*, 1979, **102**, 290.